JOURNAL of QASSIM UNIVERSITY FOR SCIENCE
©2023 Qassim University *[*E-ISSN: 1658-9610]
Vol. 2, Issue 1, pp 31-50 (July 2023)
JQUS

A First Principles Study of Transport and Magnetic Properties of PrNiBi Compound

Ahmed Elhag[1*], Abdullah Muneer S Alharbi[1]

Department of physics, college of science. Qassim University

***Correspondence author: Ahmed Elhag e-mail af.alhag@qu.edu.sa**

Abstract

We study the electronic structure and transport properties of the half-Heusler alloy PrNiBi using Density functional theory (DFT) based Full-Potential Linearized Augmented Plane Wave Method (FLAPW) within generalized gradient approximation (GGA) and generalized gradient approximation including Hubbard U-parameter (GGA + U) for the exchange correlation term of the effective Hamiltonian. Our results show that this alloy crystallizes in $C1_b$ structure with lattice parameter (a_0=6.6236Å) and maintains half metallic ferromagnetic character for a variable range of lattice parameter (6.40Å $\leq a_0 \leq$ 6.80Å) for GGA and (6.69Å $\leq a_0 \leq$ 6.76Å) for GGA+U calculation. Calculation of thermoelectric properties were carried out using semiclassical Boltzmann transport theory, in the framework of constant relaxation time approximation. It was found that the highest value of the figure of merit (ZT) correspond to carrier concentration of 2.06 per unit cell volume.

Key Words Half-Heusler, DFT, FPLAPW, electronic structure, transport properties.

1. Introduction

Rare earth (RE) containing half-Heusler (hH) alloys with chemical formula XYZ where X is a rare earth element, Y is transition metal and Z is an sp element have attracted the attention of researchers for the last decades due to their interesting thermoelectric properties along with their tunable crystal structures [1, 2]. Some of the most important properties that this family of alloys exhibit are

superconductivity [3–4], thermoelectric behavior [5], various magnetic orderings [6,7] and topological band properties [7].

Moreover, the ongoing research on half metallic ferromagnetic Heusler and half Heusler alloys have revealed that this family of alloys enjoys various functional properties with important technological application such as magnetic shape memory properties, super elasticity induced by the effect of magnetic field and large strain-induced changes in the magnetization. Such properties have attracted the attention of researches in both science and technology [8,9]. Experimental investigation on Heusler alloys of the type Ni–X–Ga, where X is a transitional element have unveiled the existence of an important effect known as ferromagnetic martensite's which is the major effect underlying the magnetic shape memory technology

Due to their unique magneto-mechanical characteristics with high efficiency, the hH alloys are considered potential candidate for different applications in magnetic sensors, magnetic recording, information storage, etc. And therefore, expected to underly promising properties for application in the emerging field of spintronics. Theoretical and NMR based studies on Bi containing hH alloys such as LnPtBi, LnPdBi and LnAuBi have indicated these compounds to be none magnetic with s-p band inversion at time reversal of momentum, whereas, ab-initio investigations indicted that the their ground states result from spin orbit coupling and therefore antiferromagnetic [10]. The electronic structure and magnetic properties of PrNiBi were studied by L. Mikaeilzadeh et al [11] using σGGA+ U approach to account for the local electron-electron interaction. The system ground state turned to be antiferromagnetic in contrast to local magnetic moment estimated by Slater-Pauling rule, this antiferromagnetism was attributed to localized 4f-electrons of the Pr atom. Furthermore, the occurrence of band inversion upon increasing the magnitude of effective Hubbard U parameter was observed. One of the most important physical problems that has been subjected to extensive investigation is the local as well as bulk magnetism of these materials. Concentration of conduction electrons along with the bonding character are the most decisive factors affecting the magnetic properties of hH alloys.

The effect of chemical bonding and electronic density of conduction electrons on magnetic ordering of full and half Heusler alloys containing transitional element have been investigated by many researchers. An important example for such studies is the one carried out by Deb,et. al, where the localized magnetism found in Cu_2MnAl alloys is strongly related to spatial distribution of d-orbitals of Mn toms [12].

Ziebeck and Webster [13] have conducted neutron diffraction, X-ray diffraction and saturation magnetization measurements on a series of found Co containing Heusler alloys. Results of their measurements show itinerant magnetism where the change in magnetic phase strongly depends on change in valence electron concentrations.

Half-metallic Heusler ferromagnets (XYZ) with energy gap in the minority spin bands and conduction electrons at the Fermi level (E_F) show 100% spin polarization and can be used as spin-polarized electron sources along with metal oxides and III–V group semiconductor nature [14]. It is known that the full-Heusler alloys such as Co_2MnZ with Z = Si, Ge demonstrate half-metallic behavior also. The magnetic properties of the Heusler alloys are very sensitive to the local geometry and chemical composition [8].

First principle DFT based techniques provide a powerful tool for investigation and understanding of crystallographic, electronic, thermoelectric and transport properties of these materials. As for many Heusler alloys such as Ni_2MnGa these properties are highly sensitive to structural variation and disorder [15]. Many approaches have been employed to theoretically investigate Ni_2MnGa, in particular augmented spherical-wave method,[15] full-potential linearized augmented-plane-wave method,[16] pseudopotential plane-wave approach,[17] etc.

Investigation of XMnSb (X=Pt, Ni) hH alloys was conducted by Youn et. al.[18] using the local spin density approximation (LSDA) have reveal a strong similarity in terms of half metallicity and magnetic properties.

Electronic structures and thermoelectric properties of rare earth containing hH alloy GdNiSb were investigated by Saini [19] Using the DFT based LSDA+U method together with classical transport theory. It was found in that the total Seebeck coefficient (S) increases linearly with temperature and attains a maximum value of 80 $\mu V\,K^{-1}$ at 800 K. The S value of 60 $\mu V\,K^{-1}$ at 380 K is in good agreement with the experimental value, 58 $\mu V\,K^{-1}$, at the same temperature. However, it was found that all the values of the thermoelectric parameters of GdNiSb indicate a good candidate for thermoelectric applications.

The major aim of this study is to investigate the electronic structure and subsequently the magnetic and transport properties of PrNiBi alloy. Since the literature on thermoelectric properties of this alloy is relatively meagre, we expect this study to pave the way for further understanding of its behavior and to establish essence for subsequent experimental and theoretical research on this and similar rare earth containing alloys. On the other hand, continuous search for materials with potential thermoelectric as well as spintronic application has motivated us to deploy DFT based techniques

as a powerful tool for estimating relevant properties. However, the LSDA method is well known for some shortcomings, in the sense that it undervalues the lattice parameters and total magnetic moments, therefore, in this work we employ the relatively more accurate GGA and GGA+U technique for our FP-LAPW investigation as implemented in WIEN2K DFT based code [20].

Quite a limited number of studies on electronic and structural properties of PrNiBi are encountered in the literature we have survived so far, while almost none has been found dealing with its thermoelectric properties. However, we have endeavored to investigate electronic and thermoelectric properties of PrNiBi, motivated by the fact that it is a hH alloy that contains rare earth together with transitional element atoms where half-metallic ferromagetism may be sought along with transport properties appropriate for thermoelectric application.

2. Materials and Methods:

In this work, first-principles calculations are carried out using the full potential linearized augmented plane wave method (FPLAPW) within generalized gradient approximation (GGA) as implemented in Vienna Ab-initio Simulation Package (WEIN2K) [20]. The generalized gradient approximation based on Perdew, Burke and Ernzerhof [21] parameterization is used to treat the electron exchange-correlation interaction part of the effective Hamiltonian. A total of 12 atoms in the unit cell with $C1_b$ structure comprising four Pr, four Ni, and four Bi atoms are considered for the self-consistency calculations. The valence electron configurations treated in calculations are $6s^2\ 4f^3$ for Pr, $3d^8 4s^2$ for Ni and $6s^2\ 6p^3$ for Bi. The total number of plane waves employed in the calculation was determined by taking the cut off energy value corresponding to $R_{MT} * K_{max} = 7.0$ (R_{MT} being the atomic radius according to muffin-tin approximation and K_{max} is the maximum amplitude of lattice vector taken for plane wave). Plane wave calculations are applied to a k-space mesh of 10×10×10 k-points in the irreducible Brillouin zone. The self-consistent cycle is considered converged when the total energy of the material is stable within 1.0×10^{-4} R_y .

we also consider the Hubbard U-correction (GGA + U) in electronic structure calculations. The effective Hubbard U parameter is defined as U_{eff}= U-J where U indicates the Coulombic part and J the exchange part of the Hubbard U energy. U_{eff} was determined by an optimization process where U_{eff} is varied until reaching the value that yields the correct magnetic moment per unit cell that is consistent with slater- Pauling rule.

Following the above-mentioned process, the optimum values of U_{eff} is 0.11 R_y for Pr f-orbitals. The effect of spin-orbit coupling was ignored in all our calculation since its effect has turned out to

be so marginal, even though the alloy contains rare earth together with heavy atom element (Bi). We have adopted GGA and GGA+U approximations according to Perdew, Burk and Ernzerhof parameterization [22].

3. Results and discussion

3.1. Structural properties

In general, the half-Heusler compounds XYZ crystallize in a zinc-blende structure where the octahedral sites are occupied, forming a face-centered cubic sub-lattice with the space group $F\bar{4}3m$. In half-Heusler compound X, Y, and Z atoms occupy the lattice fractional (0,0,0), (1/4,1/4,1/4), and (1/2,1/2,1/2) sites respectively while the (3/4,3/4,3/4) site is unoccupied [23]. Unit cell volume optimization was conducted by fitting energy versus unit cell volume data to Birch – Murnaghan equation of state. The values of cubic lattice parameter (a_0) hence obtained were a_0 = 6.6236Å for GGA approximation while for GGA +U approximation it was found that a_0 = 6.6483Å which is in a good agreement with the results of Mikaeilzadeh et. al [11] while yielding a 2.15% error with respect to the result obtained by Casper and Felser [23] using XRD-measurement.

Table.1 Cubic lattice parameter a_0 in units of Å

	Current GGA	Current GGA+U	Mikaeilzadeh et. al. [11]	Casper & Felser [23]
Current study	6.6236	6.6483	6.6443	6.5080

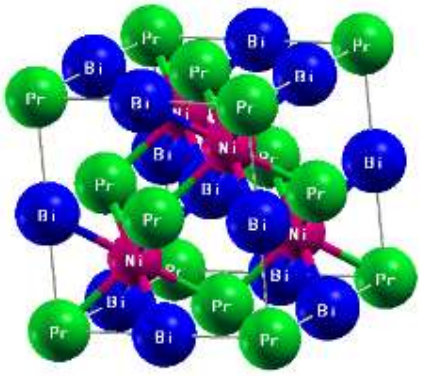

Figure.1 fcc unit cells of the half-Heusler alloy PrNiBi

3.2 Electronic properties

Electron density denotes the nature of the bonds among different atoms. In order to predict the nature of chemical bonding and the charge transfer in PrNiBi compounds, the 2D charge-density distributions have been determined for various crystal plane. Figures 2(a) and 2(b) illustrate the charge density contours for the (100) and (110) planes, respectively. Large difference (Δ) in electronegativity (ρ) is responsible for charge transfer among different atoms resulting in ionic bond nature.

For each atom in PrNiBi we have ρ(Pr) =1.33, ρ(Ni)=1.91 and ρ(Bi)=2.02 which indicate large values of Δ(Pr-Ni) and Δ (Pr-Bi) hence giving rise to (Pr- Bi) and (Pr-Ni) ionic type of bonding. This type of bonding is clearly noticed form the curvatures of contour lines and the relative magnitude of charge density in the respective interstitial regions in the tow figures while the (Ni-Bi) bond is obviously covalent and seem relatively weak due to low electron occupation in the interstitial region between atoms.

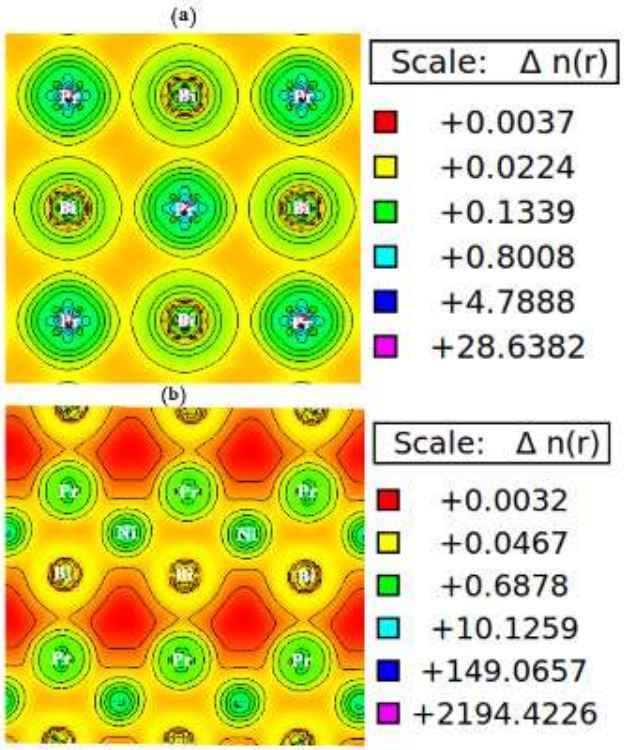

Figure.2 Spatial change density distribution in PrNiBi for (a) the (100) and (b) the (110) surfaces.

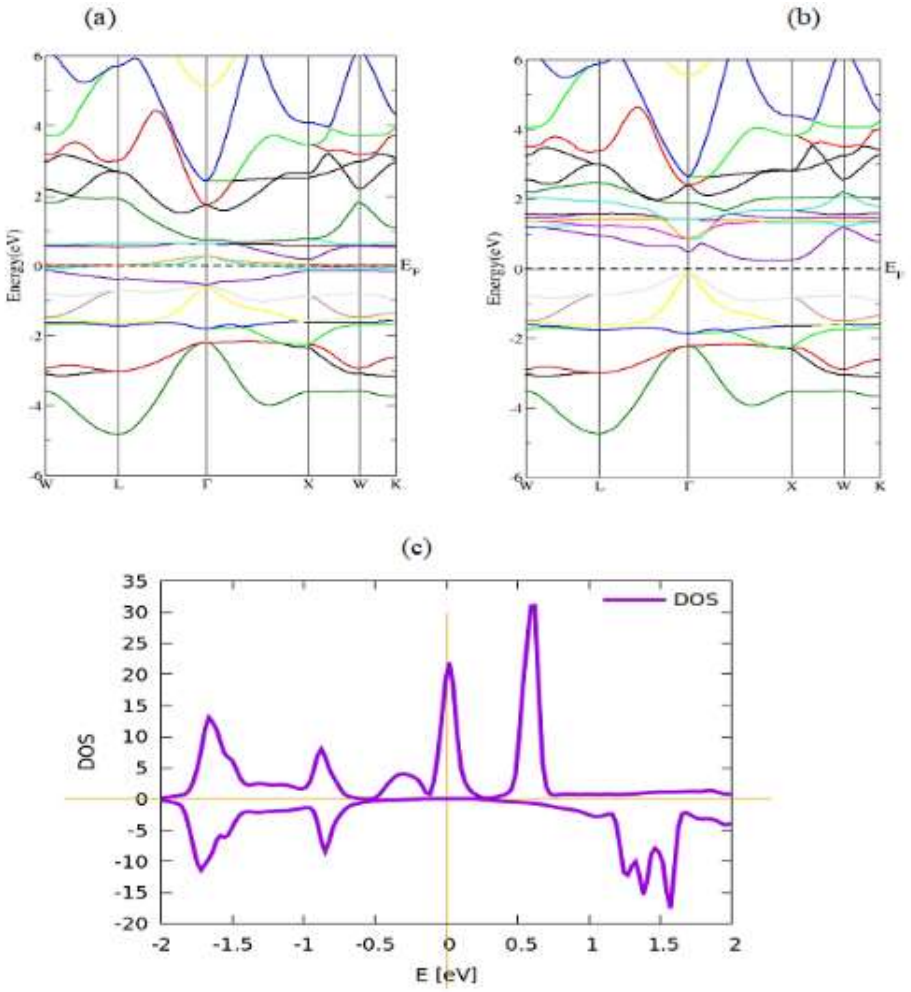

Figure.3 Band structure for PrNiBi at equilibrium lattice constant for (**a**) spin up (**b**) spin down panels and (**c**) total densities of states, as calculated using GGA approximation.

Band structures are calculated along the path WLGXWK of high symmetry points in the first Brillouin zone and presented together with total DOS in figure 3, where part (a) of the figure represents the spin majority band structure and (b) the spin minority, while the total DOS is represented in part (c). The importance of representing total DOS lies in the fact that the symmetry of the spin up and spin down DOS for spin polarized systems describes the magnetic state of the material. It is clear from figure.3.c that the total DOS is not symmetric, whether near of far from fermi level, suggesting that the ground state of the alloy is ferromagnetic. A band gap of about (≈ 0.75 eV) is observed in the spin down panel whereas no gap is there in the spin up panel, since it is clear that the Fermi level is crossed by some band as we can see in figure 4.b that this is the band formed by 4f-electron of Pr atoms. The existence of band gap in one spin direction and its absence in the other while the fermi energy level lies in the middle of that gap is an important phenomenon

called half metallicity. It is clear that the ground state of PrNiBi is a half metallic ferromagnetic. It may be noted here that we have considered the ground state corresponding to optimized lattice parameter a_0. This assertion of half metallicity is supported by band structures for both spin states displayed in parts (a) and(b) of figure.3., as Figure.3b shows an indirect band gap between the valence band maximum (VBM) at (Γ) point and the conduction band minimum (CBM) near the (X) point in the first Brillouin zone BZ.

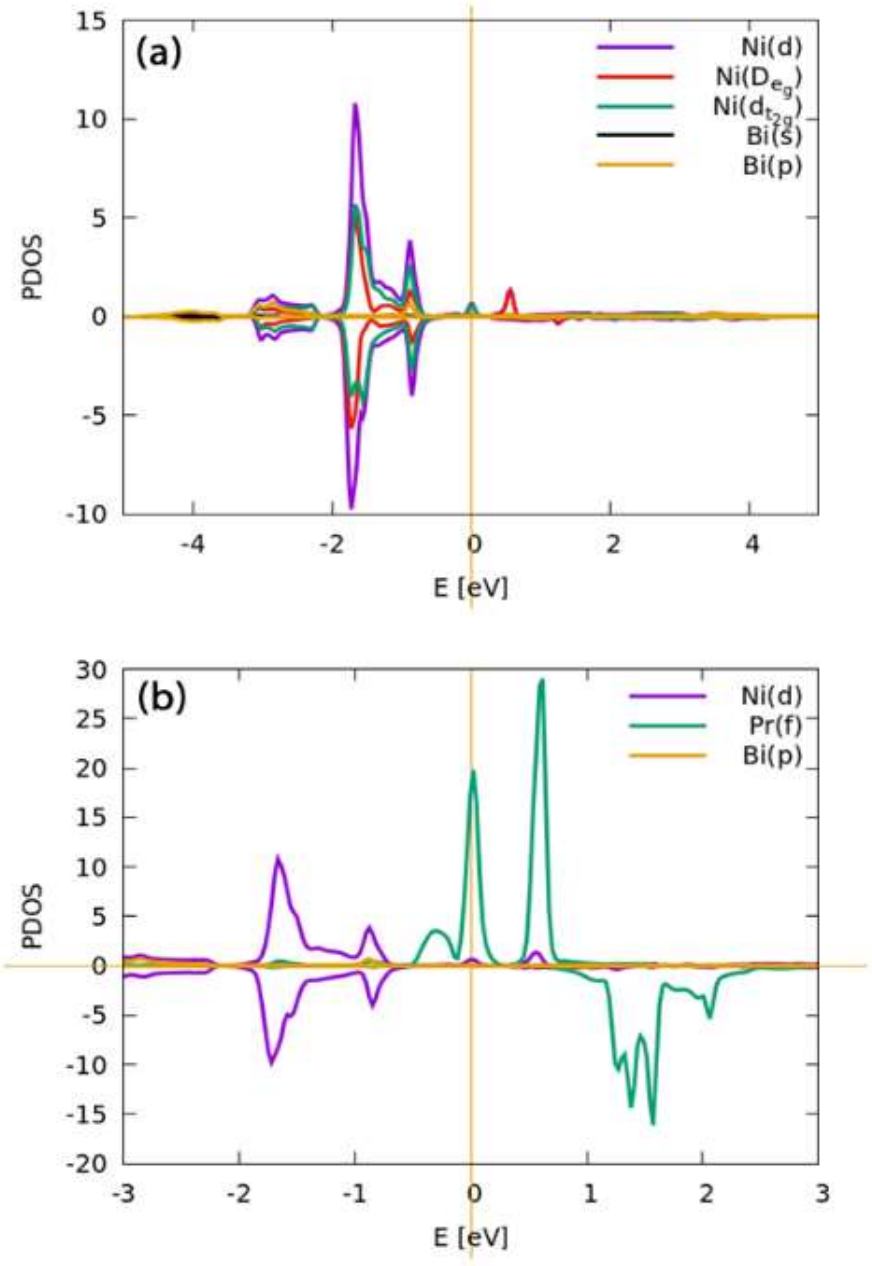

Figure.4 Partial Density of state of PrNiBi at equilibrium lattice constant (GGA).

Refering to figures.4 which depict the atomic as well as the orbital densities of states (usually called partial DOS's), we find that, in the minority (spin down) DOS, the band directly under the Fermi level is occupied by Pr(f) states. Figures.4 also show that the states responsible for half metallic behavior are the Ni(d) unoccupied states forming the CBM together with Pr f-electron occupying the VBM. Hybridization between d- electrons of Ni atoms and p or s electron of Bi atoms is yet not clearly visible.

A glance at figure.4.a shows that the occupied band extending from -2.0 eV to ~ -1.0 eV is largely populated by Ni (d-electrons) which seem unsplit by crystal field since e_g and t_{2g} orbital are strongly hybridized with each other. This phenomenon is expected as these electrons may be shielded electrostatically by s or p electron shells of the same element. Figure.4.b unveils the fact underlying the existence of the large indirect band gap in the minority spin, which is that the f-states of Pr element together with d-states of Ni are those responsible for this band gap of which the CBM is formed by Pr-f states while the VBM is formed by Ni-f states, each of which exhibits a different irreducible representation of $\bar{4}3m$ point symmetry group.

From figures.3(a) and (b) together with figures.4, we can observe that the VBM is composed of Ni(d) electrons with no apparent hybridization with Bi(s) or Bi(p) states, this is a clear indication for week bonding in the alloy. The Ni(d) states turned out to form a Γ_{15} band which is 3-fold degenerate at Γ – point (as observed in the region under fermi level in figure.3) this band splits at X-point into a Γ_{12} band which is clearly 2-fold degenerate and a Γ_1 that is non-degenerate. The Pr- f states are observed to populate the occupied valence band in the majority spin panel. These states are occupied in the majority but not in the minority which is the reason that 4f-electrons of the rare earth Pr atom are responsible for conductivity of majority spin electrons only and hence the half metallic behavior.

Cubic lattice parameters	**6.4**	**6.5**	**6.6**	**6.7**	**6.8**
Band gap	0.38	0.39	0.34	0.33	0.17
Half metallic gap	0.01	0.15	0.14	0.08	0

Table.2 Band gap and half metallic band gap vs. cubic lattice parameters (a_0) in half metallicity rage of PrNiBi.

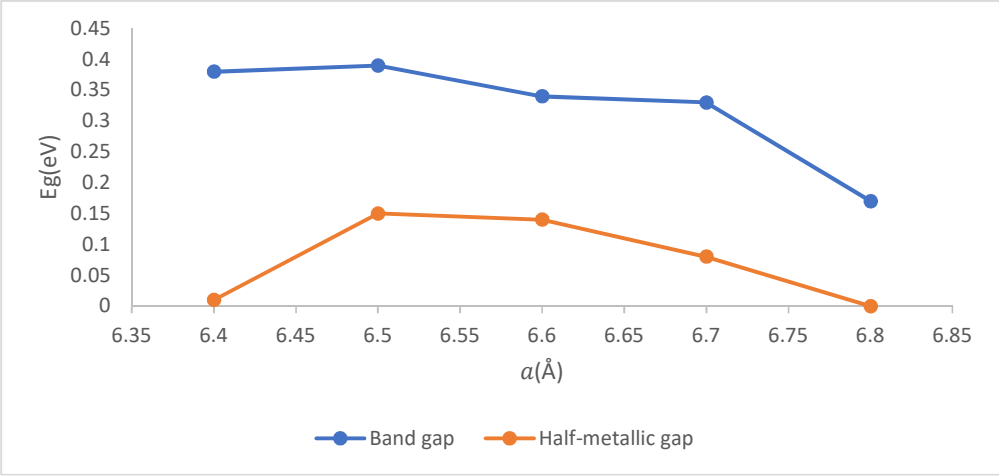

Figure.5. Half metallic gap and band gap of PrNiBi as functions of cubic lattice parameters.

The electronic band gap (in the spin minority) as well as the half metallic band gap which is the separation in the energy domain between the Fermi level and the nearest of either CBM or VBM are reported in table.1 and illustrated in figure.5 for the range of half metallicity which extends for values of cubic lattice parameter a_0 from 6.4 Å to 6.8 Å. It has been observed from figure.5 that the range of half metallicity is relatively wide as it extends for ~ 6.4Å to 6.8Å and the optimized value of a_0=6.6236Å is included within this rang. It can be seen that the HMG tends to increase in the intermediate range close to the optimized lattice parameter. Such a finding may qualifies the alloy to exhibit promising half metallic characteristics indispensable for application in spintronics.

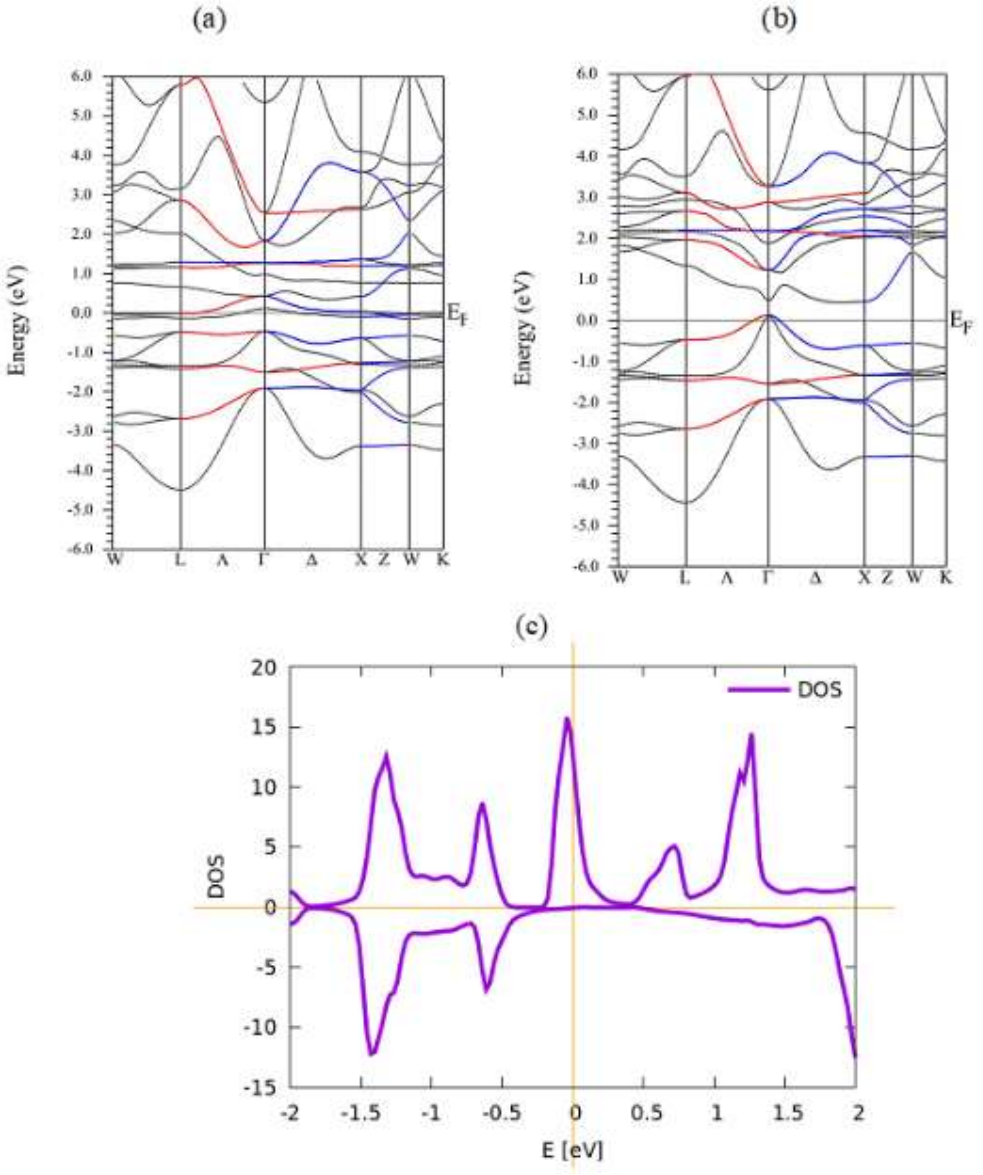

Figure.6 Band structure for PrNiBi at equilibrium lattice constant for (**a**) spin up (**b**) spin down panels and (**c**) total densities of states, as calculated using GGA +U approximation.

GGA+ U calculation results of band structure and DOS are depicted in figures (3, 4 and 6) where the band gap (minority spin) is reduced from 0.76 to 0.62 eV while the half metallic gap is sustained around 0.25 eV this effect is mainly due to upper shift in the unoccupied band above fermi level or may be due to lowering of fermi level by exchange effects. As far as the majority spin band structure with GGA + U correction is concerned, we see from figure.6 that the band composed of Ni(d) (f-electron states crosses the fermi level in the same manner as the previous case without U correction, suggesting that these states are shielded in the core prohibiting exposure to exchange effect and interaction with the crystalline environment as whole whether exchange – correlation or electrostatic

(crystal field). This assumption may explain the yet unchanging magnetic character of the alloy which as expected for rare earth containing alloys is due RE magnetic moments in the first degree.

In should be noted that the band gap has appeared to be a direct one at the Γ point with minor crossing of the Fermi level at Γ and that the occupied d states of the Ni atoms and f- states of the Pr atom are the states contributing to form the band gap. The minor crossing so observed is due to a shift in the energy position of the d- electrons. The whole picture deduced from all figure.7 is that hybridization of various states remains minimal or practically invisible may be due to week electron interaction with crystal environment.

Atomic an orbital DOS's are illustrated in figures.4,5and 7. Upon comparing these figures with corresponding ones obtained for the case of GGA calculation, we conclude that

4f electron are promoted to higher values of energies by Coulombic effects which give rise to band splitting for both the majority and minority. Ni (d)- orbitals are promoted to higher values. The effect of crystal field in terms of energy separation is not yet substantial since no $t_{2g} - e_g$ separation is not clearly observed.

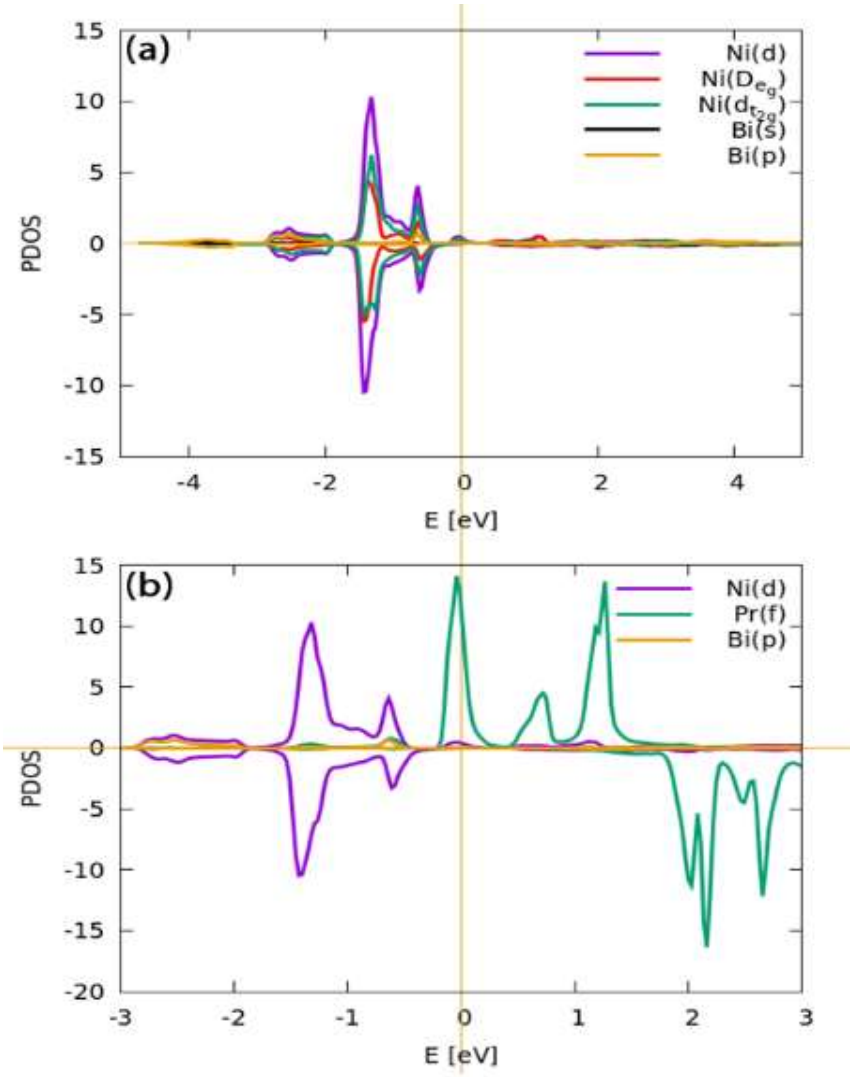

Figure.7 Partial Density of state of PrNiBi at equilibrium lattice constant (GGA+U).

d- orbitals of Ni(d) ions seem to occupy core states with very small hybridization with Bi(p)-orbitals forming a wide band extending from ~ -1.7 eV to ~ -0.5eV. U correction reveals that the exchange effects give rise to widening the band gap by pushing up the 4f electron which are expected to be responsible for that band gap. However, in conclusion, it seems that the addition of U does not lead to major changes in the general electronic structure of the compound.

3.3.Transport properties

The efficiency of thermo-electric (TE) materials is indicated by high values of the Seebeck coefficient α, and the electrical conductivity σ along with a low total thermal conductivity κ, so that for absolute temperature T, a measure for TE efficiency that is called the figure of merit ZT can be identified. ZT is a dimensionless quantity given by the form,[24].

$$ZT = \frac{\alpha^2 \sigma T}{\kappa} \qquad (1)$$

Optimization of ZT can hence be carried out by varying these parameters. Such variation can be practically achieved by varying carrier concentration in the crystal so that so that optimum values of thermal properties are obtained. This process is not as easy as it sounds since these variables are not completely independent from one another. Therefore, obtaining high values of ZT is not sufficiently performed by only adjusting one or two of these variables. To gain a broad insight into those thermo-electric properties of hH alloys, we have carried out some calculation of α, σ, and $(\kappa = \kappa_L + \kappa_e)$. such that κ_e is the electronic part and $\kappa_L$is the lattice vibrational part of the thermal conductivity, respectively. The power factor (PF), and the ZT are then calculated using the so-called constant relaxation time approximation as implemented in Boltz Trap code [25].

The chemical potential is the essential factor that determines the center of the Fermi-Dirac distribution function in energy domain. In case of electrons, the probability that a state with energy E is given by the Fermi-Dirac distribution function $f(E) = 1/(1 + exp((E - \mu)/kT))$, where μ is the chemical potential. The total number (n) of electrons per unit volume in a crystal is given the relation [26]

$$f(E) = 1/(1 + \exp(E - \mu))\, D(E)dE \qquad (1)$$

Where $D(E)$ is the density of states at energy E, so that the total number of electron per unit volume is given by

$$n = \int_0^\infty f(E, T, \mu)\, D(E)dE \qquad (2)$$

In equation (2), the density of states $D(E)$ is given according to the Fermi-Dirac distribution function f(E, T, μ). Equation (2) determines the relation between the chemical potential and electron concentration for at temperature (T). For $((E - \mu)/kT) \gg 1$ which is the classical limit for Fermi-Dirac distribution, the Boltzmann distribution function can be used so that

$$n = N_c(T)\exp\left(\frac{-(E_c - \mu)}{kT}\right) \qquad (3)$$

Where N_c is the density of states at the edge of conduction band given by $N_c = \left(\frac{2\pi mkT}{h}\right)^{\frac{3}{2}}$.

Equation (3) is used to determine the electron chemical potential in doped semiconductors [26]

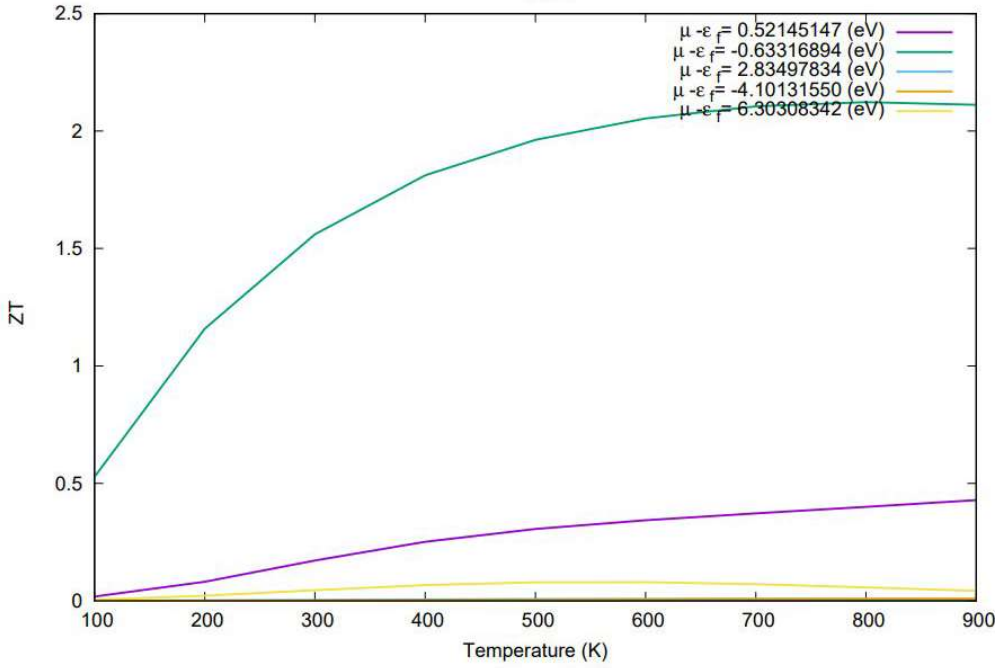

Figure.8 The figure of merit (ZT) versus temperature for different values of the parameter $\boldsymbol{\delta}$

In **Figure.8**. the figure of merit ZT for PrNiBi alloys is represented as a function of temperature (T) for different values of the difference $\boldsymbol{\delta}$ between chemical potential μ and Fermi energy E_F . From this figure we can observe that ZT increases with temperature in different manners depending on the value of $\boldsymbol{\delta}$. This is of course not an unexpected behavior for a function that depends on interrelated quantities as we have preceded. The value of $\boldsymbol{\delta}$ that continuously renders the highest set of value (highest curve) of ZT is $\boldsymbol{\delta}$ = -0.63316894 eV. ZT for this value steadily increases with temperature to reach a saturation limit ($ZT \approx 2.1$) at a high temperature range of T > 700 K. The value of $\boldsymbol{\delta}$ is related to the carrier concentration (n) via equation (3), where $\boldsymbol{\delta} =$ μ- E_F, μ is the chemical potential and E_F is Fermi energy

Optimal value of the carrier concentration (the one corresponding to $\boldsymbol{\delta}$ = -0.63316894 eV) was calculated. It was that is $n = 2.06/\Omega$, where Ω is the unit cell volume. Needless to mention that the results so far obtained has much to do with thermal conductivity, since from (1), high values of ZT are obtained for low thermal conductivities. Figure 9 represents the variation of conductivity (κ)

with temperature. It is clearly observed thereby that the lowest thermal conductivity corresponds to $\boldsymbol{\delta} = -0.63316894$ eV, which is the value that gives rise to high ZT.

From figure 8 and 9, we find that at **δ**= -0.63316894 eV, the figure of merit (ZT) renders high value, while the electronic thermal conductivity κ takes the lowest set of values (lowermost curve).

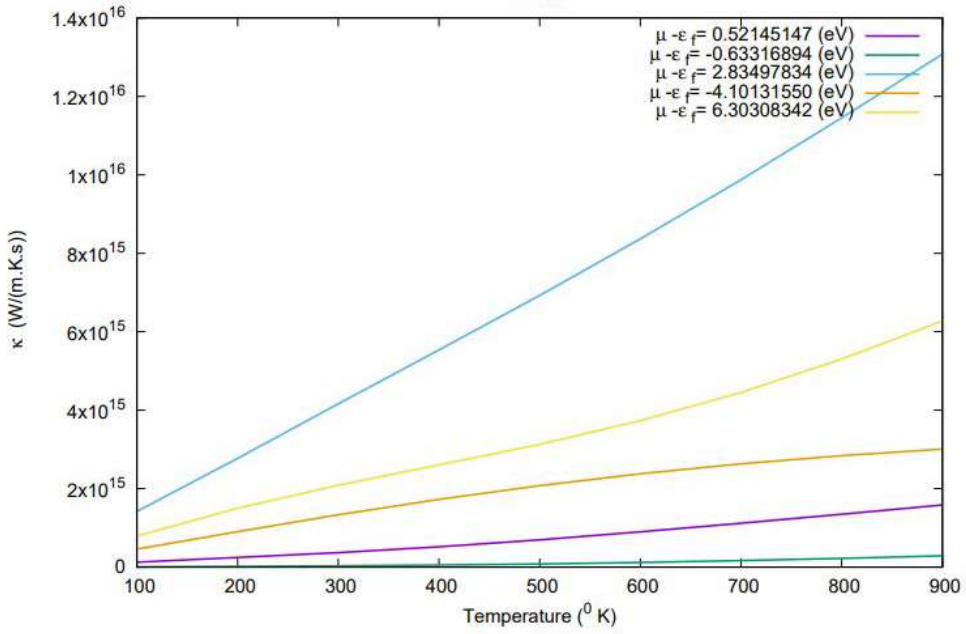

Figure.9 Thermal conductivity of PrNiBi versus temperature for different values of the parameter ***δ***

Another important thermoelectric property is the power factor (PF) which is defined by the relation PF = $\alpha^2\sigma$. PF as a function of temperature for different values of **δ** is represented in figure.10. By comparing figure.9 with 10, it is noticeable that the value of **δ** (-0.63316894 eV) which gives rise to higher curve of ZT does not necessarily correspond to higher PF set of values. For this specific value (**δ**) the PF almost varies linearly with T, so that if the PF is the quantity to be tuned apart from optimal figure of merit (ZT) the selection of **δ** will then depend on which operational range of temperature is chosen since a value of **δ** =2.83497834eV**.** Will give rise to highest PF curve in the range T < ~ 670 and δ= -0.63316894 eV for T > 670 K.

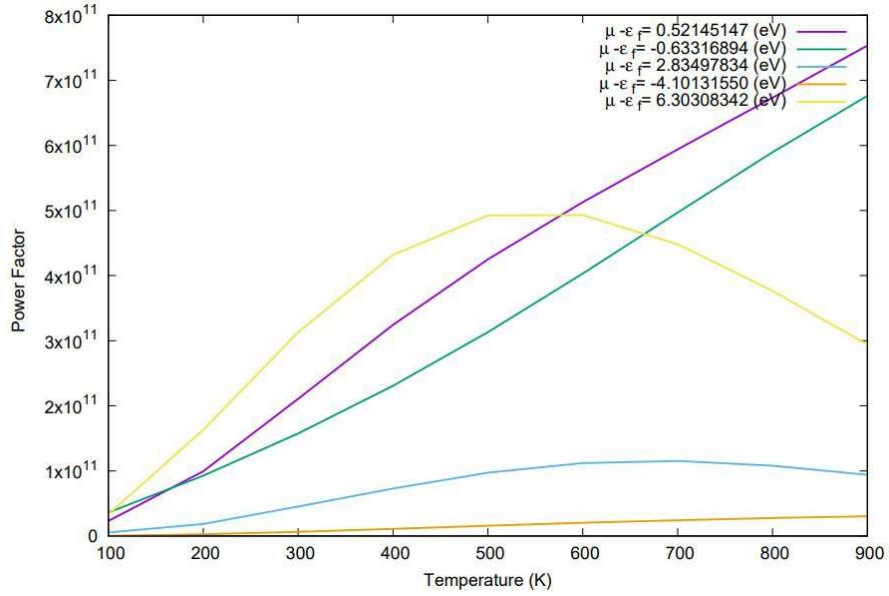

Figure.10 The Power factor versus temperature for different values of the parameter ***δ***

Figure.11 show the Seebeck coefficient (α) as a function of temperature, the linear relation between α and *ZT* has imposed a similar behavior in temperature range of the study so that for a high value of Seebeck for all temperature from 0 to 900 K the values **δ** = -0.633169 eV are the ones to deal with.

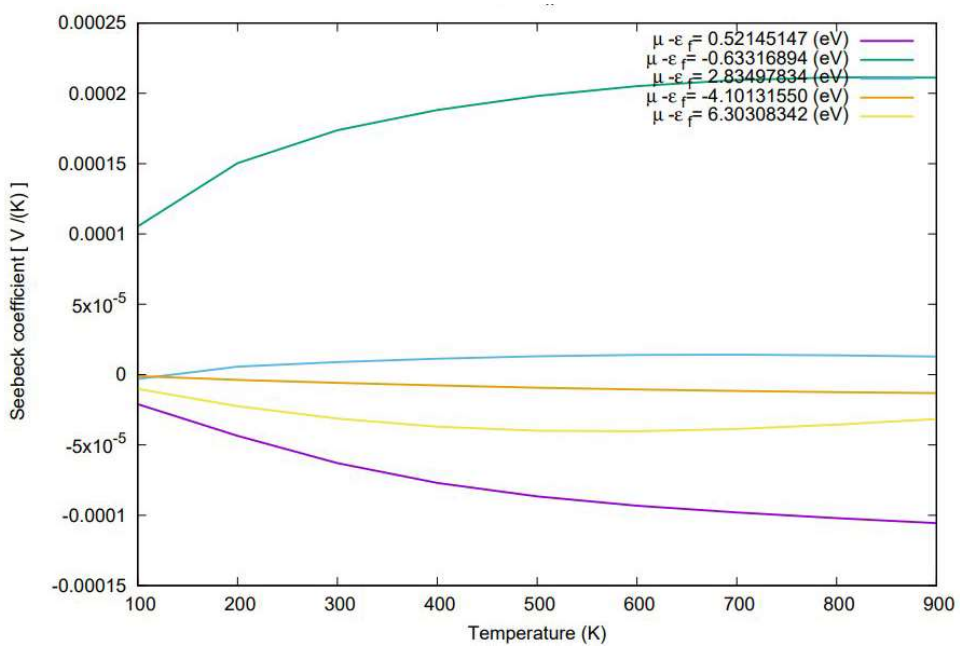

Figure.11 The Seebeck coefficient versus temperature for different values of the parameter δ

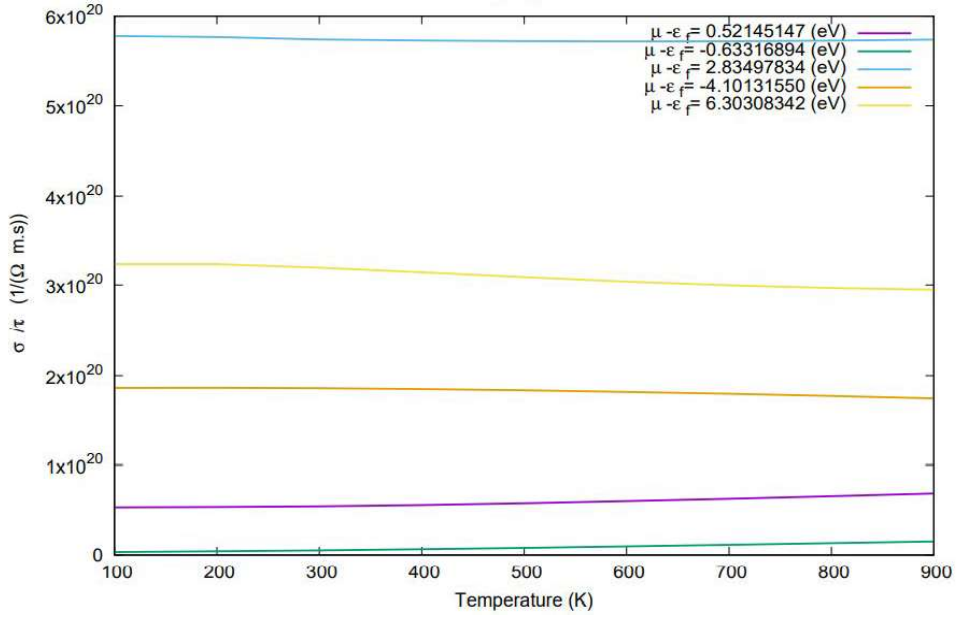

Figure.12 The electrical conductivity (σ) of PrNiBi versus temperature for different values of the parameter δ

Although the figure of merit is high, the value of the electrical conductivity is low for the same chemical potential μ- E_F = -0.63316894 eV, and slowly increases with temperature as is depicted in figure.12. Relatively small electric conductivity (σ) should limit the thermoelectric efficiency of the alloy.

Conclusion:

In the present work, we have investigated the structural, electronic and transport properties of the half-Heusler alloy PrNiBi using first-principle calculations based on the FP-LAPW method. Two approximations were used to treat the exchange correlation potential: GGA and GGA+U approximations. Variation of energy per unit cell volume was fitted to Birch-Murnaghan equation of state to for both ferromagnetic (FM) and nonmagnetic (NM) ground states. The structural analysis reveals that the ferromagnetic is the most stable ground state of the studied material. The results of the electronic properties unveil a half-metallic behavior for tunable cubic lattice parameter a ranging from [6.40Å to 6.80Å]. Thermoelectric properties (ZT, α, σ, κ and PF) were calculated for a range of temperature from 0 to 900 K. The values obtained indicated high figure of merit and electric conductivity for chemical potential (μ =0.02) for the whole range of temperature covered by the study. This finding gave rise to required carrier concentration $n = 2.06/\Omega$ that allows highest power factor values and consequently a better thermoelectric efficiency.

References:

1. J. Tobola, J. Pierre, S. Kaprzyk, R. Skolozdra, and M. A. Kouacou, Crossover from semiconductor to magnetic metal in semi-Heusler phases as a function of valence electron concentration, Journal of Physics: Condensed Matter, 10 1013, 1998.
2. A. Tavana and L. Mikaeilzadeh, A frst principles study of iron doping in Ni_2CoGa magnetic shape memory alloy, AIP Advances, 5 117210, 2015.
3. Xu, Guizhou, W. Wang, X. Zhang, Y. Du, and E. Liu, Weak antilocalization efect and noncentrosymmetric superconductivity in a topologically nontrivial semimetal LuPdBi, Scientifc reports, 4 5709, 2014.
4. S. M. A. Radmanesh, Evidence for unconventional superconductivity in half-Heusler YPdBi and TbPdBi compounds revealed by London penetration depth measurements, Physical Review B, 98 241111, 2018.
5. J. Yang, , H, Li, T. Wu, W. Zhang, L. Chen and J. Yang, Evaluation of half-Heusler compounds as thermoelectric materials based on the calculated electrical transport properties, Advanced Functional Materials, 18 2880, 2008.
6. P avlosiuk, O. Kaczorowski, D., Fabreges, X. Gukasov and P. Wiśniewski, Antiferromagnetism and superconductivity in the half-Heusler semimetal HoPdBi, Scientifc reports, 6 18797, 2016.
7. Y. Nakajima, R. Hu, K. Kirshenbaum, A. Hughes, P. Syers, X. Wang and J. Paglione, Topological RPdBi half-Heusler semimetals: A new family of noncentrosymmetric magnetic superconductors. Science advances, 1 1500242, 2015.
8. S. E. Kulkova, S. V. Eremeev, T. Kakeshita, S. S. Kulkov and G. E. Rudenski, The electronic structure and magnetic properties of full-and half-Heusler alloys, Materials transactions, 47 3 ,2006.
9. S. E. Kulkova, S. V. Eremeev and S. S. Kulkov, Electronic structure and magnetic properties of Co-and Mn-based Heusler alloys and thin films, Solid state communications, 13012, 2004.
10. Mong, R. S. K., Essin, A. M. & Moore, J. E. Antiferromagnetic topological insulators, Physical Review B, 81 245209, 2010.
11. L. Mikaeilzadeh, A. Tavana an F. Khoeini, Electronic structure of the PrNiBi half-Heusler system based on the σGGA + U method, Sci Rep., 9- 20075, 2019.
12. A. Deb and Y. Sakurai, Electronic structure of the Cu_2MnAl Heusler alloy, Journal of Physics: Condensed Matter, 12 13, 2000.
13. K. R. A. Ziebeck, and P. J. Webster, A neutron diffraction and magnetization study of Heusler alloys containing Co and Zr, Hf, V or Nb, Journal of Physics and Chemistry of Solids, 35 1, 1974.
14. Y. Sakuraba1, S. Kokado, Y. Hirayama, T. Furubayashi, H. Sukegawa, S. Li1, Y. K. Takahashi, and K. Hono, Quantitative analysis of anisotropic magnetoresistance in Co_2MnZ and Co_2FeZ epitaxial thin films: A facile way to investigate spin-polarization in half-metallic Heusler compounds, Applied Physics Letters, 104 17, 2014.
15. J. Kübler, R. William and C. B. Sommers, Formation and coupling of magnetic moments in Heusler alloys, Physical Review B, 28 4, 1983.
16. S. E. Kulkova, S. V. Eremeev and S. S. Kulkov, Electronic structure and magnetic properties of Co-and Mn-based Heusler alloys and thin films, Solid state communications, 130 12, 2004.
17. V. V. Godlevsky and K. M. Rabe, Soft tetragonal distortions in ferromagnetic Ni2 MnGa and related materials from first principles, Physical Review B, 63 13, 2001.
18. S. J. Youn and B. I. Min, Effects of the spin-orbit interaction in Heusler compounds: Electronic structures and Fermi surfaces of NiMnSb and PtMnSb, Physical Review B, 51 16, 1995.

19. S. M. Saini, Electronic Structure and Thermoelectric Performance of Narrow-Gap GdNiSb Half Heusler Compound: Density Functional Calculations, Physica Status Solidi 258, 4 2000491, 2021.
20. P. Blaha, K. Schwarz, G, K. Madsen, D. Kvasnicka, and J. Luitz, WIEN2k, An Augmented Plane Wave + Local Orbitals Program for Calculating Crystal Properties, Techn. Universitat Wien, Austria ISBN: 3-9501031-1-2, 2001.
21. L. Shuhui, A new half-metallic ferromagnet La2NiFeO6: predicted from first-principles calculations, The Journal of Physical Chemistry C, 114 39, 2010.
22. M. Fadila and C. Belkharroubi, Structural, magnetic, electronic and mechanical properties of full-Heusler alloys Co2YAl (Y= Fe, Ti): first principles calculations with different exchange-correlation potentials, Journal of Magnetism and Magnetic Materials, 448, 2018.
23. F. Casper, and C. Felser, Magnetic and Electronic Properties of RENiBi (RE= Pr, Sm, Gd–Tm, Lu) Compounds, Zeitschrif für anorganische und allgemeine Chemie, 634 2418, 2008.
24. T. M. Tritt, Thermoelectric phenomena, materials, and applications, Annual review of materials research, 41 1, 2011.
25. G. Madsen, K. H.Georg and David J. Singh, BoltzTraP. A code for calculating band-structure dependent quantities, Computer Physics Communications, 17 1, 2006.
26. A.Jayaraman, Abhijit Bhat Kademane, and M. Muralikrishna, DFT Study on the Carrier Concentration and Temperature-Dependent Thermoelectric Properties of Antimony Selenide , Indian Journal of Materials Science, 7296847, 2016.